Bearing Multi-Faults Diagnosis Based on Stator Current Bi-spectrum Features and Support Vector Machines

Lotfi Saidi[1,2], Chakib Ben Njima[3,4], Abdelaziz Lakehal[5]

[1] *University of Tunis, ENSIT – Laboratory of Signal Image and Energy Mastery, Tunisia*
[2] *University of Sousse, Higher School of Sciences and Technology of Hammam Sousse- Tunisia*
[3] *University of Monastir, ENIS- Laboratory of Automatic Signal and Image Processing, Tunisia*
[4] *University of Sousse, Higher Institute of Transport and Logistics of Sousse, Tunisia*
[5] *University of Souk-Ahras, LRESF laboratory, Algeria*
lotfi.saidi@ieee.org; *chakib.bennjima@enim.rnu.tn; a.lakehal@univ-soukahras.dz*

***Abstract*—This paper presents a novel pattern classification approach for bearings diagnostics, which combines the higher order spectra analysis features and support vector machine classifier. The stator current bi-spectrum patterns are extracted as the feature vectors presenting different faults of the bearings. These features were fed to a support vector machine to distinguish six kinds of fault-bearing signals which were measured in the experimental test bench running under different working conditions. The results indicated that the proposed method can reliably identify different fault patterns of rolling element bearings based on the stator current signals.**

Keywords—Bi-spectrum analysis, feature extraction, multi-fault classification, rolling element bearing, principal component analysis, support vector machine.

I. INTRODUCTION

As a critical component, rolling element bearings (REB) are widely used in induction motors (IMs). Bearings are required to run with high reliability, and the occurrences of faults may lead to fatal breakdowns of IMs [1, 2]. It is well known that bearing defects (BDs) represents one of the most common sources of faults in IMs (about 40%-50%) [3-10]. Therefore, it is significant to accurately detect and diagnose the existence and severity of the faults occurring in the REB.

Traditionally, diagnostics of bearings is carried out using monitoring of the bearing vibration signals [5-6, 10-12]. This method requires the use of accelerometers or other vibration sensors and appropriate devices for signal conditioning and can be expensive and not always simple to be performed [13].

Usually, if any fault occurred in IMs through one or more failed components, it will affect the behavior of the stator current [10]. Contrary to vibration signals, monitoring of stator current requires the use of a current probe that can also be employed for the diagnosis of other types of faults [3].

Motor current signature analysis (MCSA) has been developed to perform condition monitoring and faults diagnosis of IMs. A brief review of MCSA was highlighted in [8, 9, 15]. When the early fault occurs, the REB characteristic frequencies contain very little energy and the background noise is very important so that the characteristic fault frequencies are usually buried in the noise and higher levels of macro-structural vibrations. However, bearing faults cannot be directly identified using traditional MCSA techniques [15, 16]. For several decades both the first and second-order statistics, such as mean, variance, autocorrelation, and power spectrum [17, 1] are popular signal processing tools and have been used extensively for MCSA. However, they are subject to describing linear and Gaussian processes. Or, in practice, most of the situations with nonlinear and non-Gaussian behaviors can be conveniently studied using advanced signal processing techniques, such as higher-order statistics (HOS). The advantages of these methods are [15-19],

- Features are not affected by Gaussian noise,
- Can exploit non-Gaussianity and non-linearity in signals,
- Can obtain information about phase relations in signals.

Relatively, only a few papers discussed the application of HOS analysis (HOSA) in IMs fault diagnosis. Even though many researchers have performed fault detection of IMs using MCSA but they do not perform the diagnosis and identification of multiple faults. For these reasons, this paper tries to contribute to the use of stator current bi-spectrum (third-order spectrum) analysis for multi-fault BDs diagnosis.

Motivated by the HOS advantages, this paper presents a novel pattern classification approach for BDs diagnostic, which combine the bi-spectrum analysis features and support vector machine (SVM) classifier. The stator current bi-spectrum patterns are extracted as the feature vectors presenting different BDs. The SVM algorithm is adopted to distinguish six kinds of BDs signals which were measured in the experimental test bench running under different working conditions with the removal of varying speed and load (or torque) dependence.

In the area of machine learning classification technologies, artificial neural networks (ANN) has fast development in the past several years [10-14], which impels its development in fault diagnosis research and application. Generally, ANN has some problems such as identification ability difference, structure identification difficulty, no standard method to determine the structure of the network, local convergence, and other issues. SVM can better solve these problems [10, 11], so it achieves better decision accuracy in special cases because of the maximized decision boundary, and it is efficient for large datasets and real-time analysis [10].

In IMs fault diagnosis, some researchers have employed SVM as a tool for the classification of faults. For example, in

[6] a wind turbine gearbox fault diagnosis method based on diagonal spectrum and clustering binary tree SVM, has been proposed. The fault features are extracted by the diagonal spectrum. Then the clustering binary tree is used to classify the fault categories.

In [2] SVM is used along with continuous wavelet transform. The results obtained are hoped to set up a base for the condition monitoring technique of IMs which will be simple, fast, and overcome the limitations of traditional techniques. The main drawback of this technique is the problem to determine the optimal parameters for the wavelet filter.

In [11] fault detection of REB using SVM and ANN is presented. The vibration signals are collected to analyze the bearing condition, which has four faults: inner race fault, outer race fault, ball fault, and cage fault. Statistical features based on moments and cumulants are used and the optimal features are selected using a genetic algorithm. In the classification process, SVM is employed using radial basic kernel function (RBF) with constant kernel parameters.

The remainder of this paper is organized as follows. The basic principles of the bi-spectrum and its derived features are discussed in Section 2. Section 3 presents the proposed method, including the description of the data preprocessing procedure, the selected feature set, and the proposed multi-SVM-based classifier. Section 4 presents the experimental results including a description of the experimental test bench and the paper concludes in Section 5.

II. BI-SPECTRUM AND FEATURES DERIVED FROM THE BI-SPECTRUM

A. Brief description of bi-spectrum

The bi-spectrum belongs to the class of HOS, used to represent the frequency content of a signal. HOS provides higher-order moments and nonlinear combinations of the higher-order moments called cumulants [16-17]. An overview of the theory of HOS can be found in [16-17].

The bi-spectrum can be estimated directly from the discrete Fourier transform (FT) of M realization of the sampled version of the non-Gaussian third-order stationary and ergodic IMs stator current $x(t)$ as follows [16, 17];

$$\begin{aligned}\hat{B}(f_1,f_2) &= \frac{1}{M}\sum_{i=1}^{M} X_i(f_1)X_i(f_2)X_i^*(f_1+f_2) \\ &\approx E\left\{X(f_1)X(f_2)X^*(f_1+f_2)\right\}\end{aligned} \tag{1}$$

where f_1, f_2 are the frequency indices, X^* denotes the complex conjugate of X and $X(f)$ is the FT of the discrete signal $x(n)$ and $E\{.\}$ is an average over an ensemble of realizations of a random signal.

It can be noted that the bi-spectrum presents twelve symmetry regions [15-19]. Hence, the analysis can take into consideration only a single non-redundant region. Hereafter, $B(f_1, f_2)$ will denote the bi-spectrum in the triangular region τ defined by:

$$\tau = \left\{(f_1,f_2) : 0 \le f_2 \le f_1 \le f_e/2, f_2 \le -2f_1 + f_e\right\} \tag{2}$$

where f_e is the sampling frequency.

In the next section, the composition of the extracted and selected features dataset is further discussed.

B. Features extraction and reduction

❖ Features extraction

This paper proposes to use the following derived bi-spectrum features from the stator's current bi-spectrum, which are presented as follows [22]:

i. The sum of logarithmic amplitudes of the bi-spectrum:

$$F_1 = \sum_{f_1,f_2\in\tau} log\left(\left|B(f_1,f_2)\right|\right) \tag{3}$$

ii. The sum of logarithmic amplitudes of diagonal elements in the bi-spectrum is calculated as:

$$F_2 = \sum_{f_k\in\tau} log\left(\left|B(f_k,f_k)\right|\right) \tag{4}$$

iii. The first-order spectral moment of amplitudes of diagonal elements in the bi-spectrum:

$$F_3 = \sum_{f_k\in\tau} k.log\left(\left|B(f_k,f_k)\right|\right) \tag{5}$$

iv. The normalized bi-spectral entropy:

$$P_1 = -\sum_n p_n log(p_n) \tag{6}$$

where $p_n = \dfrac{\left|B(f_1,f_2)\right|}{\sum_{f_1,f_2\in\tau}\left|B(f_1,f_2)\right|}$

v. The normalized bi-spectral squared entropy:

$$P_2 = -\sum_n q_n log(q_n) \tag{7}$$

where $q_n = \dfrac{\left|B(f_1,f_2)\right|^2}{\sum_{f_1,f_2\in\tau}\left|B(f_1,f_2)\right|^2}$

vi. The bi-spectrum phase entropy (P_e) [22]:

$$P_e = \sum_n p\psi_n \log(p\psi_n) \tag{8}$$

where

$$p\psi_n = \frac{1}{L}\sum_{\tau} 1(\phi(B(f_1,f_2)) \in \Psi_n \tag{9}$$

and, 1(.) is an indicator function that gives a value of 1 when the phase angle ϕ is within the range of bin Ψ_n in Eq. (10).

$$\psi_n = \left\{\phi \mid -\pi + \frac{2\pi n}{N} \le \phi < -\pi + \frac{2\pi(n+1)}{N}\right\}, \tag{10}$$

$n = 0,1,...,N-1$

L is the number of points within the non-redundant region given by (2), ϕ refers to the phase angle of the bi-spectrum, and

vii. The weighted center of bi-spectrum (WCOB) [22] is given by

$$WCOB_1 = \frac{\sum_{\tau} iB(i,j)}{\sum_{\tau} B(i,j)} \tag{11}$$

$$WCOB_2 = \frac{\sum_{\tau} jB(i,j)}{\sum_{\tau} B(i,j)} \tag{12}$$

where i and j are the frequency bin index in the non-redundant region expressed in (2).

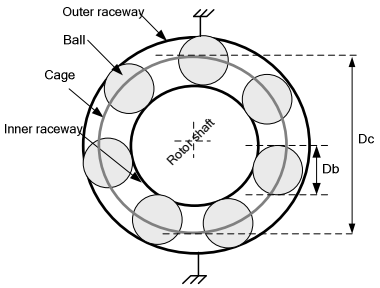

Fig. 1. Fig.1. Geometry of REB.

Then the features vector is expressed as,

$$T = \left[F_1, F_2, F_3, P_1, P_2, P_e, WCOB_1, WCOB_2\right] \quad (13)$$

In the next section, principal component analysis (PCA) is introduced to eliminate correlations between features and reduce the dimensionality of the original feature vectors.

❖ Features reduction

Feature reduction means transforming the original features into a lower-dimensional space. Most feature extraction techniques have based on linear techniques such as principal component analysis (PCA). PCA is a quantitatively rigorous method for achieving data dimensionality reduction. The method generates a new set of variables, called principal components (PCs), which maximizes the variance of the projected vectors. Each PC is a linear combination of the original variables. All the PCs are orthogonal to each other, so there is no redundant information. The PCs as a whole form an orthogonal basis for the space of the data. Thus, the first PC consists of the highest variability; the second PC consists of the next highest variability, and so on for other directions.

III. BEARINGS MULTI-FAULT CLASSIFICATION PROPOSED METHOD

A. Bearing defects (BDs) signatures

Failure surveys [8, 9] by the Electric Power Research Institute (EPRI) indicate that IMs bearing-related faults are about 40% of the most frequent faults in IMs [2-5], [8, 9]. As shown in Fig. 1, the bearings consist mainly of the outer and inner raceways, the balls, and the cage. BDs can be classified into two classes: single-point defects and generalized roughness [3, 5]. Single-point defects are localized and classified into,

- Outer raceway defect;
- Inner raceway defect;
- Ball defect.

Generalized roughness is a type of fault where the condition of a bearing surface has degraded considerably over a large area and become rough, irregular, or deformed. These faults may enhance vibration and noise levels [3]. Moreover, there are internal operating stresses caused by vibration, eccentricity, and bearing current. Additionally, bearings can also be affected by other external causes such as:

- Contamination and corrosion;
- Lack of lubrication causing heating and abrasion;
- Defect of bearing's mounting, by improperly forcing the bearing onto the shaft or in the IM's stand.

TABLE I. REB PARAMETERS USED IN THE EXPERIMENTAL SETUP.

Type	Outside diameter	Inside diameter	N_b	D_b	D_p	cosβ
SKF 6004	42 *mm*	20 *mm*	9	6,35*mm*	31*mm*	1

The single-point defect may be seen by fault frequencies appearing in the machine vibration spectrum record. The frequencies at which these components occur are predictable and depend on the surface on which the bearing contains the fault. Therefore, there are different fault frequency characteristics associated with each component among the four parts of the bearing [3].

These frequencies are: f_I: inner race fault frequency, f_O: outer race fault frequency, f_C: cage fault frequency, and f_B: ball fault frequency, their mathematical equations are as follows:

$$f_O = \frac{f_r}{2} N_b \left(1 - \frac{D_b \cos\beta}{D_c}\right) \quad (14)$$

$$f_I = \frac{f_r}{2} N_b \left(1 + \frac{D_b \cos\beta}{D_c}\right) \quad (15)$$

$$f_C = \frac{f_r}{2} \left(1 - \frac{D_b \cos\beta}{D_c}\right) \quad (16)$$

$$f_B = \frac{f_r}{2} \frac{D_c}{D_b} \left[1 - \left(\frac{D_b \cos\beta}{D_c}\right)^2\right] \quad (17)$$

where,

f_r : rotor shaft frequency
N_b : number of rolling elements
D_b : ball diameter
D_c : pitch diameter
β : ball contact angle

However, these characteristic race frequencies in Eqs. (14) and (15) can be approximated for most bearings with between six and twelve balls by [3]

$$f_O = 0.4 N_b f_r \quad (18)$$

$$f_I = 0.6 N_b f_r \quad (19)$$

The torque oscillations generate stator current components at predictable fault-bearing frequencies. The bearing fault frequencies f_{Bng} are related to the oscillations and electrical supply frequency by [3, 4]

$$f_{Bng} = \left| f_s \pm m f_v \right| \quad (20)$$

Where f_s is the power supply frequency, f_v is one of the characteristic vibration frequencies (f_C, f_O, f_I, f_B), and m= 1, 2, 3, …

Table I shows the parameters of the bearing used in our experimental test bench (Fig. 6), taken from the datasheet.

B. BDs stator current bi-spectrum: a theoretical approach

In this section, the BDs bi-spectrum stator current signal is theoretically presented. This theoretical analysis will be also confirmed by some experimental results.

A simulated signal is built to testify to the proposed method.

Let us consider that the stator current is given by Eq. (21). This signal is similar to the measured current for an inner race

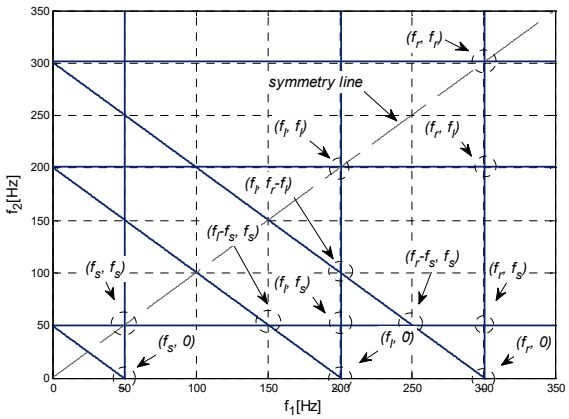

Fig. 2. Graphical illustration of stator current bi-spectrum given in Eq. (22), where the bi-spectrum peaks are indicated by arrows.

fault at rated speed (2780 rpm), and rated torque, thus accordingly to Eq. (15), f_v = 251.12 Hz. This signal is generated at a sampling rate of 4096 Hz. Assume the simplest case of a stator current signal, where only the first sideband frequencies associated with the BDs (f_l=$|f_s$-$f_v|$=201.12 Hz. And f_r =$|f_s$+$f_v|$= 301.12 Hz) are considered. Here index *l* for left, and index *r* for right, in absolute values.

$$i_a(t) = i_f \cos(2\pi f_s t - \varphi) + i_l \cos(2\pi f_l t - \varphi_l) + i_r \cos(2\pi f_r t - \varphi_r) \quad (21)$$

with

i_f : RMS value of the supply phase current

i_l, φ_l : RMS value of the lower current component at f_l= $|f_s$-$f_v|$, and its phase angle respectively

I_r, φ_r : RMS value of the upper current component at f_r= $|f_s$+$f_v|$, and its phase angle respectively

φ : Phase angle at the supply frequency

By ignoring contributions of negative frequencies which fall outside the useful region of interest given in expression (2), the bi-spectrum of the stator current signal generated by BDs is theoretically calculated using the Fourier transform of expression (21) and substituted in the bi-spectrum formula given by (1), is given by (22):

$$\begin{aligned} B(f_1,f_2) &= I_a(f_1)I_a(f_2)I_a^*(f_3 = f_1 + f_2) \\ &= \frac{1}{8}\begin{pmatrix} i_f\delta(f_1 - f_s)e^{j\varphi} + i_l\delta(f_1 - f_l)e^{j\varphi_l} \\ + i_r\delta(f_1 - f_r)e^{j\varphi_r} \end{pmatrix} \times \\ &\quad \begin{pmatrix} i_f\delta(f_2 - f_s)e^{j\varphi} + i_l\delta(f_2 - f_l)e^{j\varphi_l} \\ + i_r\delta(f_2 - f_r)e^{j\varphi_r} \end{pmatrix} \times \\ &\quad \begin{pmatrix} i_f\delta(f_3 - f_s)e^{-j\varphi} + i_l\delta(f_3 - f_l)e^{-j\varphi_l} \\ + i_r\delta(f_3 - f_r)e^{-j\varphi_r} \end{pmatrix} \end{aligned} \quad (22)$$

Where δ(.) represents the Dirac delta function.

By plotting $B(f_1,f_2)$ in the bi-spectrum domain as shown in Fig. 2 and 3, it can be seen that each of the three factors consists of three parallel delta function lines (f_i=f_j, where i=1,2,3 and j=*l,s,r*). Therefore, the non-redundant region of computation of the bi-spectrum $B(f_1,f_2)$ is non-zero at twelve points (peaks in the bi-spectrum) shown in Fig. 2.

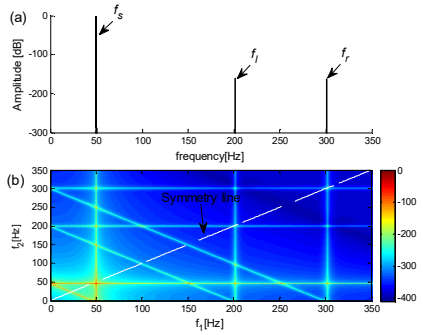

Fig. 3. (a) Stator current power spectrum, and (b) its bi-spectrum displayed as color images, associated with the current signal given in Eq. (21).

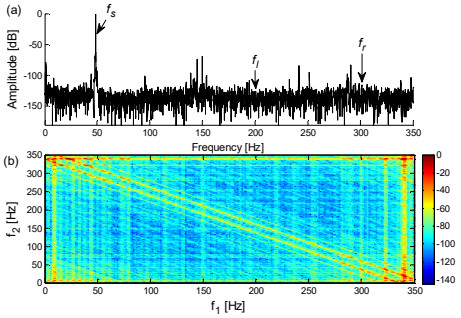

Fig. 4. (a) Zoomed stator current power spectrum and (b) its bi-spectrum displayed as color images, IM running at rated speed and rated torque condition; this is to be compared with the results in Fig. 2 and Fig. 3.

Eq. (22) shows that every stator current signal generates a bi-dimensional bi-spectral pattern characterized by peak positions shown in Figs. 2 and 3. The energy distribution in the bi-spectrum domain is validated experimentally by the analysis of real stator current induction motor recorded using a test bench shown in Fig. 4. Fig. 4 (b) shows the bi-spectrum of stator current with inner race fault at rated speed sampled at f_e= 10 kHz, in the frequency bandwidth [0, 350 Hz].

C. Support vector machine (SVM)

❖ Binary SVM

SVM is a binary classifier developed by Vapnik, which performs IMs fault detection using its superior capacity in the classification process. Based on the input data vectors that consist of IMs fault features, SVM will identify these patterns.

Furthermore, binary SVM can be extended to multi-class. This is the subject of the next Subsection.

❖ Multiple classes SVM

As mentioned above SVMs were originally designed for binary (2 classes) classification [6, 10-12, 23]. In binary classification, the class labels can take only two values: 1 and -1. In the real problem, however, we deal with more than two classes for example: in condition monitoring of IMs, there are several classes such as mechanical unbalance, misalignment, different load conditions, bearing faults, gear faults, etc. Therefore, multi-class SVM is obtained by decomposing the multi-class problem into several binary-class problems. The multi-class classification methods will be discussed in [10, 23].

TABLE II. BINARY ENCODING FOR EACH BDS.

	SVM1	SVM2	SVM3	SVM4	SVM5
IRF	+1				
ORF	-1	+1			
BF	-1	-1	+1		
IOBF	-1	-1	-1	+1	
GIOF	-1	-1	-1	-1	+1
HB	-1	-1	-1	-1	-1

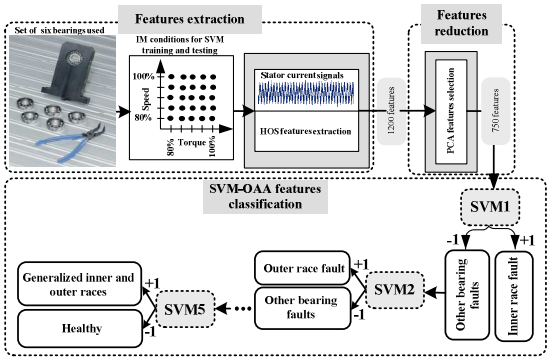

Fig. 5. Proposed diagnostic methodology for multi-faults diagnosis scheme based on SVM-OAA classifier.

Two different approaches are taken into account: one-against-all (OAA) and one-against-one (OAO) [10, 23]. In the first one, the *i-th* SVM is trained with all the examples in the *j-th* class with positive labels and all the other examples with negative labels, while in the latter one, each classifier is trained on data from two classes. Here, SVM-OAA is chosen to classify different bearing faults.

We do not make comparisons SVM-OAA strategy with other popular approaches like SVM-OAO in this paper, because of the following reasons:

- ✓ Benchmark comparisons on multiclass SVM approaches already exist in the literature [23].
- ✓ It has been concluded [23] that SVM-OAA is as accurate as any other approach, assuming that all underlying binary SVMs are well-tuned.

The training procedure and choice of SVM parameters for training are very important for classification. In this work, the process of optimizing the SVM parameters with the cross-validation method is adopted.

D. BDs classification based on SVM

The diagram of the fault diagnosis scheme is presented in Fig. 5. The procedure of the proposed method can be summarized as follows:

Step 1: Data acquisition.

Step 2: Signal processing.

Step 3: Bi-spectrum features.

Step 4: Bi-spectrum features reduction using the PCA method.

Step 5: Classification process for fault diagnosis by SVM-OAA based on multi-faults classification. Since only six bearing conditions need to be identified in this paper, just five SVM classifiers need to be designed, as indicated in Fig.5, and Table II. For SVM1, define the inner race fault (IRF) condition as y= +1, and the remaining 5 other conditions, as another class, identified as -1, thus the IRF could be separated from other conditions by SVM1. Then define the condition with outer race fault (ORF) as y= +1 and the other conditions as y= -1 for SVM2, thus the ORF could be separated from other conditions by SVM2. Similarly, the ball fault (BF) could be separated from other conditions by SVM3 and so on, until the classification test is completed. Then they become a multi-class fault diagnosis system as shown in Fig. 5. Note that all the five SVMs adopt RBF as their kernel function. We choose the RBF for the SVM classifier since previous studies have shown that it has the best performance in pattern recognition tasks. As well, the RBF kernel is a better choice than other kernels like polynomial kernel because it has lesser hyper-parameters and so the problem becomes less computationally intensive. SVM-OAA algorithm is used, furthermore, some parameters are predefined for this classifier such as the regularizing parameter C and the kernel parameter γ are set to 100 and 0.5 respectively, which were selected based on the cross-validation method.

I. EXPERIMENTAL RESULTS: APPLICATION OF THE PROPOSED METHOD IN BDS

A. Description of the experimental setup and data acquisition

The test rig shown in Fig. 6 (a) was composed of a variable speed of 0.37 kW IM at 2780 rpm of rated speed controlled by an inverter, driving a shaft rotor and a controlled brake, assembly through flexible couplers; shafts were rested on two ball bearings. The bearings under analysis were placed at the load end side for ease of replacement. The BDs were carried out during the manufacture. A milling cutter was used to scratch the corresponding surfaces. The test rig was used for modeling different fault types such as eccentricities, misalignment, and different types of BDs. Stator current signals were collected using a 16-bit A/D converter at a sampling rate of 10 KS/s. The numbers of samples collected were one hundred thousand for a duration of 10 s.

To take into account different speed and torque combinations, 25 measurements for each bearing condition are considered: from 80% to 100% rated speed, and from 80% to 100% of rated torque, every variation of 5% of each parameter.

The bearing data set was obtained from the experimental test rig under six different operating, where six identical bearings (SKF6004) have been used covering the most important BDs scenarios: (a) HB (25 measurements), (b) with an ORF (25 measurements), (c) with an IRF (25 measurements), (d) with a BF (d) with an inner and outer race as well as ball bearing faults (IOBF) (25 measurements) and (f) with generalized inner and outer races degradation (GIOF) (25 measurements).

The SVMs training experiments are conducted on a data set (150 current signals, including 25 signals for six different bearing conditions). The classification results are shown in Table III, Table IV, and Table V.

To show the effect of the speed and torque on the bi-spectrum features distribution we take as an example the normalized bi-spectrum entropy values for the 25 acquisitions in each condition are evaluated, presented in Fig. 7. This plot

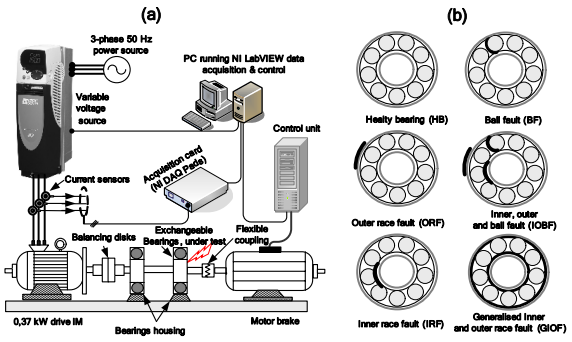

Fig. 6. (a): The instrumentation of the experimental set-up for BDs detection, and (b): A series of bearing components with faults induced in them indicated in bold line.

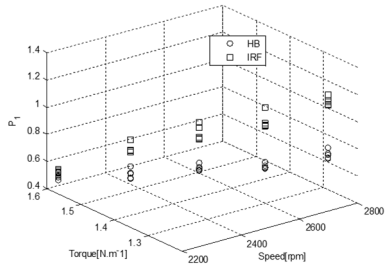

Fig. 7. The effect of speed and torque on statistically normalized bi-spectral entropy parameters distribution.

shows how this parameter is influenced by the speed and the torque both for the healthy and damaged case and it increases with higher speeds. Moreover, it can be noticed that in low-speed cases this parameter value for the damaged bearing is almost near to the healthy one when it reaches the highest speed.

Fig. 8 (left side) represents the original features (P_1, P_2, P_e) that are not well clustered and have a disordered structure. Plotting original feature parameters indicates the necessity of preprocessing the original features to make them separable and ready for classification. The disordered structure of original features tends to decrease the performance of the classifier if it is directly processed in the classifier.

To avoid this disadvantage, PCA was proposed to extract and reduce the feature dimensionality based on the eigenvalue of the covariance matrix. Therefore, the first five principal components have been selected to replace the original feature vector.

Fig. 9 shows the feature reduction in component analysis based on eigenvalues of the covariance matrix. The axes of the projection plane correspond to the maximum variance directions in the initial space. As shown in Fig. 8 (right side), the number of features is reduced from 8 to 5.

B. Training and test vectors

The training and testing of the SVM model with real-time data sets were implemented with the help of LIBSVM software [23]. The total databases comprised 1200; (25×6×8) original features. The number of features is reduced to 750; (25×6×5) selected features, were divided into two sets: one for training (containing 60% of the samples), and the other for the

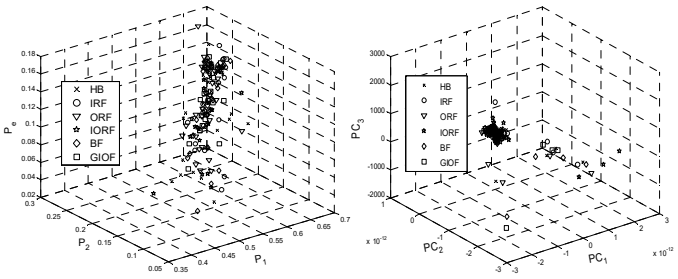

Fig. 8. Distribution of "P_1", "P_2" and "P_e" features of (left) original data features, (right) original features obtained from PCA.

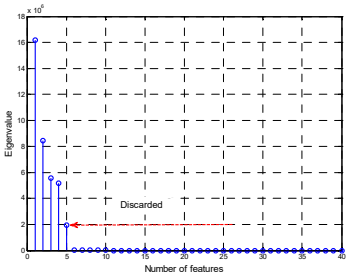

Fig. 9. Eigenvalues of the covariance matrix for feature reduction.

test (containing 40% of the samples). After the SVM is trained with 450 features, its performance has been tested with the 300 remainings (50 features for each BDs).

The performance of the SVM-OAA is validated by calculating the classification accuracy (CA) performance measure for the train set and test set separately.

$$CA[\%] = \frac{number\ of\ correctly\ classified\ samples}{total\ number\ of\ \ samples\ in\ dataset} \times 100 \qquad (23)$$

The classification results of all classifiers in the training and testing processes are presented in Table VI. In the training process, all the SVM-OAA classifiers achieve an average accuracy of 99.165% and 99.331% in the whole dataset and the reduced dataset, respectively, some of them without any misclassification out of 450 samples (respectively 720 samples) of training data for all bearing features. This indicates that the classifiers are well-trained and can be applied for diagnosing BDs. However, in the testing process these classifiers are validated against the test data, the average accuracy is about 96% and 95.416% for the reduced and original features respectively. The miss- classifications are due to the overlap of machine condition features.

A confusion matrix is a useful tool for analyzing how well the classifier can recognize tuples of different groups, which contains information about actual and predicted classifications done by a classification system.

From the confusion matrix of the SVM in Table III and Table IV and Table V, one can note that SVM finds it difficult to discriminate between GIOF and IRF, ORF, BF. A Miss classification of 4% brings down the diagnostic ability of the SVM-OAA; however, the overall classification accuracy is reasonably good. It can be seen that the BF presented the highest accuracy of 100%.

From the test results shown in Table III, Table IV, and

Table V it can be seen that the SVM-OAA classifiers recognize the defect samples effectively, especially for the HB signals, IRF signals, and ORF signals. The recognition results of SVM are ideal because of its high accuracy and good generalization capability when the average classification efficiency is close to 96% is reasonably good.

TABLE III. CONFUSION MATRIX FOR THE MULTICLASS SVM-OAA RESULTING FROM THE EVALUATION OF THE WHOLE DATASET.

		Predicted					
		HB	**IRF**	**ORF**	**BF**	**IOBF**	**GIOF**
Actual	**HB**	78	0	2	0	0	0
	IRF	1	79	0	0	0	0
	ORF	3	1	74	0	0	2
	BF	0	0	0	80	0	0
	IOBF	0	2	3	1	72	2
	GIOF	0	3	1	0	1	75

TABLE IV. CONFUSION MATRIX FOR THE MULTICLASS SVM-OAA RESULTING FROM THE EVALUATION OF THE REDUCED DATASET.

		Predicted					
		HB	**IRF**	**ORF**	**BF**	**IOBF**	**GIOF**
Actual	**HB**	49	0	0	0	0	1
	IRF	1	49	0	0	0	0
	ORF	1	1	47	0	0	1
	BF	0	0	0	50	0	0
	IOBF	0	2	1	1	46	0
	GIOF	0	1	1	0	1	47

TABLE V. THE TESTING ACCURACY* FOR SIX DIFFERENT BEARING CONDITIONS USING SVM-OAA

Bearing conditions	**SVM including all features**		**SVM including selected features**	
	Classification accuracy [%]		**Classification accuracy [%]**	
	Training	**Testing**	**Training**	**Testing**
HB	99.16	97.50	100	98.00
IRF	100	98.75	100	98.00
ORF	100	92.50	100	94.00
BF	100%	100	100	100
IOBF	98.33	90.00	97.33	92.00
GIOF	97.5	93.75	98.66	94.00
Average	99.165	95.416	99.331	96.00

*Accuracy is computed based on the confusion matrix provided in the paper.

II. CONCLUSION

In this work, an effort is made to characterize and classify six different REB classes depending on their bi-spectrum features. A flexible test bed was created and current signals were taken for six different bearing conditions at different speeds and torque conditions. The best CA of six conditions of bearing was 100% on the test set for the OAA-SVM. The results show that the OAA-SVM is a strong technique for fault diagnosis of rotating machinery. Also, the results demonstrate the ability of the proposed combination "HOS-SVM" model in diagnosing REB failures.

REFERENCES

[1] Lei Y G, He Z J, Zi Y Y. Fault diagnosis of rotating machinery based on multiple ANFIS combination with Gas. Mech Syst Signal Process, 2007; 21(5): 2280-94.

[2] Konar P, Chattopadhyay P. Bearing fault detection of induction motor using wavelet and Support Vector Machines (SVMs). Appl Soft Comput, 2011; 11: 4203-11.

[3] Frosini L, Bassi E. Stator current and motor efficiency as indicators for different types of bearing faults in induction motors. IEEE Trans. Ind. Electron, 2010; 57(1): 244-51.

[4] Saidi L, Fnaiech F, Capolino G-A, Henao H. Stator current bi-spectrum patterns for induction machines multiple-faults detection. In Proc IEEE IECON, ÉTS, Montréal, Canada, 2012, 5132-37.

[5] Lee J, Ghaffari M, Elmeligy S. Self-maintenance and engineering immune systems: Towards smarter machines and manufacturing systems. Annual Reviews in Control, 2011; 35: 111-22.

[6] Wenyi L, Zhenfeng W, Jiguang H, Guangfeng W, Wind turbine fault diagnosis method based on diagonal spectrum and clustering binary tree SVM. Renewable Energy, 2013; (50):1-6.

[7] L.Saidi, J.Ben Ali, F.Fnaiech,"Bi-spectrum based-EMD applied to the non-stationary vibration signals for bearing faults diagnosis," *ISA Transactions,* 53. pp.1650-660, 2014.

[8] L.Saidi, F.Fnaiech, J.Ben Ali, "Application of higher order statistics and support vector machines for bearing faults classification," *ISA Transactions*, 2015, 54, pp. 193-206.

[9] J.Ben Ali, L.Saidi, A.Mouelhi, B.Chebel-Morellob, F.Fnaiech,"Linear feature selection and classification using PNN and SFAM neural networks for a nearly online diagnosis of bearing naturally progressing degradations", *Engineering Applications of Artificial Intelligence,* 2015, 42, pp. 67-81.

[10] Widodo A, Yang B-S. Support vector machine in machine condition monitoring and fault diagnosis. Mech Syst Signal Process; 2007; 21: 2560-74.

[11] Jack L B, Nandi A K. Fault detection using support vector machines and artificial neural network, augmented by genetic algorithms. Mech Syst Signal Process, 2002; 16 (2-3): 373-90.

[12] Gryllias K C, Antoniadis I A. A support vector machine approach based on physical model training for rolling element bearing fault detection in industrial environments. Engineering Applications of Artificial Intelligence, 2012; 25: 326-44.

[13] Delgado M, Cirrincione G, Espinosa A G, Ortega J A, Henao H. Bearing faults detection by a novel condition monitoring scheme based on statistical-time features and neural networks. IEEE Trans. Ind. Electron, 2013; 30(8): 3398-7.

[14] Ramirez A-G G, G, Osornio-Rios R A, Lieberman D G, A. G. Perez; R. J R. Troncoso. Smart sensor for online detection of multiple-combined faults in VSD-fed induction motors. Sensors, 2012; 12, (9): 11989-5.

[15] Saidi L, Fnaiech F, Capolino G-A, Henao H. Diagnosis of broken bars fault in induction machines using higher order spectral analysis. ISA Transactions, 2013; 52: 140-8.

[16] Nikias C L, Petropulu A, Higher-Order Spectra Analysis: A nonlinear signal processing framework, 1993; Englewood Cliffs, New Jersey: Prentice-Hall.

[17] Mendel J M. Tutorial on higher order statistics (Spectra) in signal processing and system theory: theoritical results and some applications. Proceedings of the IEEE; 1991; 79: 287-5.

[18] Courtney C R P, Neild S A, Wilcox P D, Drinkwater B W. Application of the bispectrum for detection of small nonlinearities excited sinusoidally. Journal of Sound and Vibration, 2010; 329: 4279-93.

[19] Zhou Y, Chen J, Dong G M., Xiao W B, Wang Z Y. Application of the horizontal slice of cyclic bispectrum in rolling element bearings diagnosis. Mech Syst Signal Process, 2012; 26: 229-43.

[20] LIBSVM-A Library for Support Vector Machines. Available from: http://www.csie.ntu.edu.tw/~cjlin/libsvm.

[21] Yiakopoulos C T, Antoniadis I A. Cyclic bispectrum patterns of defective rolling element bearing vibration response. Forsch Ingenieurwes, 2006; 70: 90-4.

[22] Chua K C, Chandranb V, Acharyaa U R, Lima C M. Application of higher order statistics/spectra in biomedical signals-A review. Medical Engineering & Physics, 2010; 32(7): 679-89.

[23] Rifkin R, Klautau A, In Defence of One-Vs.-All Classification. Journal of Machine Learning, 2004; 5: 101-141.